Ma *et al. Microstructures* 2024;4:2024012
DOI: 10.20517/microstructures.2023.60

Microstructures

Research Article

Open Access

Pressure-induced superconductivity in $SnSb_2Te_4$

Yanmei Ma[1], Hongbo Wang[1], Ruihong Li[1], Han Liu[1], Jian Zhang[1], Xianyu Wang[2], Qiang Jing[2,3], Xu Wang[1], Wenping Dong[1], Jinman Chen[1], Bingze Wu[1], Yonghao Han[1], Dan Zhou[4,5], Chunxiao Gao[1]

[1]State Key Laboratory of Superhard Materials, College of Physics, Jilin University, Changchun 130012, Jilin, China.
[2]Laboratory of Functional Molecules and Materials, School of Physics and Optoelectronic Engineering, Shandong University of Technology, Zibo 255000, Shandong, China.
[3]Key Laboratory of Artificial Structures and Quantum Control (Ministry of Education), Shanghai Jiao Tong University, Shanghai 200240, China.
[4]Department of Materials Science, College of Materials Science and Engineering, Jilin University, Changchun 130012, Jilin, China.
[5]School of Physics, Changchun University of Science and Technology, Changchun 130022, Jilin, China.

Correspondence to: Prof. Yanmei Ma, State Key Laboratory of Superhard Materials, College of Physics, Jilin University, Changchun 130012, Jilin, China. E-mail: ymma@jlu.edu.cn; Prof. Jian Zhang, State Key Laboratory of Superhard Materials, College of Physics, Jilin University, Changchun 130012, Jilin, China. E-mail: zhang_jian@jlu.edu.cn; Assoc. Prof. Qiang Jing, Laboratory of Functional Molecules and Materials, School of Physics and Optoelectronic Engineering, Shandong University of Technology, 266 Xincun Xi Road, Zibo 255000, Shandong, China; Key Laboratory of Artificial Structures and Quantum Control (Ministry of Education), Shanghai Jiao Tong University, Shanghai 200240, China. E-mail: jingqiang@sdut.edu.cn; Assoc. Prof. Dan Zhou, Department of Materials Science, College of Materials Science and Engineering, Jilin University, Changchun 130012, Jilin, China; School of Physics, Changchun University of Science and Technology, Changchun 130022, Jilin, China. E-mail: zhoudan@cust.edu.cn

How to cite this article: Ma Y, Wang H, Li R, Liu H, Zhang J, Wang X, Jing Q, Wang X, Dong W, Chen J, Wu B, Han Y, Zhou D, Gao C. Pressure-induced superconductivity in $SnSb_2Te_4$. *Microstructures* 2024;4:2024012. https://dx.doi.org/10.20517/microstructures.2023.60

Received: 18 Oct 2023 **First Decision:** 11 Dec 2023 **Revised:** 22 Dec 2023 **Accepted:** 11 Jan 2024 **Published:** 27 Feb 2024

Academic Editors: Zhi-Gang Chen, Shujun Zhang **Copy Editor:** Fangling Lan **Production Editor:** Fangling Lan

Abstract
Owing to their unique compositional and structural characteristics, layered van der Waals solids in binary and ternary chalcogenide families provide a fertile testbed for exploring novel exotic structures and states, e.g., topological insulators and superconductors. Herein, a comprehensive study on the structural variations and correlated electrical transport behavior of $SnSb_2Te_4$, a ternary member, has been carried out considering elevated pressures. Under 45.6 GPa, three distinct structural phase transitions have been observed, with strong evidence from the variations of high-pressure X-ray diffraction patterns. The onsets of phase II (monoclinic, *C2/m*) at 6.3 GPa, phase III (monoclinic, *C2/c*) at 15.5 GPa, and phase IV (body-centered cubic with substitutional disorder, *Im-3m*) at 17.2 GPa have been observed owing to the emergence of new diffractions. Based on electrical measurements at low temperature and high pressure conditions, two pressure-induced superconducting states

have been distinguished in $SnSb_2Te_4$. The first state occurs in the range of 12.3-17.1 GPa. The positive pressure dependence on *Tc* indicates that the aforementioned state is related to the monoclinic *C2/m* phase. At > 17.1 GPa, the second superconducting state emerges, with the negative pressure dependence on *Tc*. It relates to the body-centered cubic solid solution phase, which is characteristic of a substitutional disordered crystal structure. The discovery that the pressure-induced superconductivity in $SnSb_2Te_4$ is affected by structural phase transitions under pressure may help understand the universal relationship between the ambient condition topological insulating state and derived superconductivity. *Ab initio* theoretical calculations reveal that an electronic topological transition takes place at approximately 2.0 GPa, which is featured by the obvious changes in the distribution of electronic density of states near the Fermi level.

Keywords: Superconductivity, structural phase transitions, topological insulators, high pressure, diamond anvil cell

INTRODUCTION

The pursuit of new superconductors and the comprehension of the superconductivity mechanism constitute one of the most active forefront subjects in condensed matter physics and materials science[1-4]. The recent discovery of topological superconductors (TSs) has introduced new concepts in the family of superconductors and elucidated the superconducting mechanism. TSs are bulk superconductors; however, they exhibit spin-polarized metallic topological surface states. Therefore, the transport properties of materials with topological features, including but not restricted to topological insulators and TSs, have attracted considerable research interest. Based on both the theoretical simulations[5,6] and the experimental measurements[7,8], typical layered ternary chalcogenides, AB_2X_4 (A = Ge, Sn, and Pb; B = Sb and Bi; X = Se and Te), have been recognized as topological insulators under ambient conditions. $GeBi_2Te_4$, $SnSb_2Te_4$, and $SnBi_2Te_4$ (and their parent binary counterparts, e.g., Sb_2Te_3[9], Bi_2Te_3[10], and Bi_2Se_3[11]) have been considered as promising TS candidates.

These binary or ternary chalcogenide compounds have been intensively studied. They comprise a flexible and versatile system to develop new applications and explore the relationship of various ordered states. Moreover, the compounds exhibit extraordinary thermoelectric[12], galvanomagnetic, and thermomagnetic properties[13,14] and novel and exotic phenomena, such as electronic topological transition (ETT), metal-insulator transition, topological quantum phase transition, structural phase transition, and superconductivity[15-18]. While crystalizing in a similar tetradymite-like layered structure, ternary topological compounds, i.e., AB_2X_4, possess the advantage (over their binary counterparts) of tuning their structures and properties based on the appropriate selection and substitution of atoms in the A site. Specifically, $SnSb_2Te_4$ acts as an intrinsic p-doped 3D TI with a narrow indirect Eg band gap of approximately 0.1 eV. Based on the angle-resolved two-photon photoemission measurement combined with the density functional theory (DFT) calculations about the electronic energy band structure, the Dirac cone is observed at 0.32 eV above the Fermi level[19]. High-pressure techniques have played an important role in tuning the superconducting states and the electronic properties of materials[20-23]. For $SnSb_2Te_4$, the pressure-induced superconducting transition occurs at 8.1 GPa with an onset T_c value of approximately 2 K[22]. With a further increase in pressure, T_c increases monotonously, indicating the pressure-induced enhancement of superconductivity. However, a subsequent study indicates that $SnSb_2Te_4$ tends to decompose into its constituent binary compounds (α-Sb_2Te_3 and SnTe) at medium high pressures (> 7 GPa)[20]. Thus, the observed superconductivity at higher pressures needs to be investigated to exclude the interference of the high pressure phases of the binary constituents. Moreover, other layered ternary chalcogenides, such as $SnBi_2Se_4$, $GeSb_2Te_4$, and $PbBi_2Te_4$[15,22,24-26], have been reported to undergo complicated but sequential superconducting transitions under compression. The characteristic superconducting transition parameters, such as T_c and P_c, vary considerably. However, in these homologous materials, pressure-induced decomposition into corresponding binary constituents has not been reported to date. From this perspective, the stability and phase transition of $SnSb_2Te_4$ and related layered ternary chalcogenides need to be investigated.

To address the aforementioned problem and clarify the evolution of the structures and electronic transport features of $SnSb_2Te_4$ under compression, we have conducted systematic experimental studies combined with theoretical simulations on $SnSb_2Te_4$ at elevated pressures. The observation of pressure-induced superconductivity is confirmed at pressures above approximately 12.3 GPa with variable critical temperatures. Superconductivity is enhanced at the initial pressure range, and the maximum superconductivity is achieved at 8.2 K (T_c) and 17.1 GPa. After that, a kink appears in the *Tc-P* plot. The sharp reduction and negative pressure dependence of T_c at higher pressures suggest the presence of a second superconducting state. Moreover, it is revealed by the high pressure synchrotron X-ray diffraction (XRD) studies that the initial *R-3m* structure transforms to a *C2/m* phase (phase II) at 6.3 GPa, a nominal phase III at 15.5 GPa, and a substitutional alloy (phase IV, *Im*-3*m*) at 17.2 GPa. The consistency in the critical pressures of the structural and superconducting transitions indicates that the two high pressure superconducting states are closely correlated to the pressure-induced structural transitions in $SnSb_2Te_4$.

EXPERIMENTAL AND CALCULATION DETAILS

Sample preparation and characterization

The coarse-grained single crystals of $SnSb_2Te_4$ were prepared by a self-flux synthetic route. Powders of the elements Sn, Sb, and Te with a purity better than 99.99% were used as purchased (Aladdin Company, China). They were mixed together according to the expected atomic ratio (Sn:Sb:Te = 1:2:4). The initial reactants were ground vigorously in an agate mortar to turn them into a homogenous mixture. The mixture was then transferred into a quartz ampule. The ample was evacuated and sealed to ensure airtightness. The temperature of the ampule was raised to 950 °C at a heating rate of 40 °C per hour. The high temperature transformed the reactants into a melting flux and induced reactions among them. Afterward, the temperature of the ampule was lowered to 500 °C at a rate of 20 °C per hour. The products were annealed at this temperature for four days. At last, the power supply was turned off, and the temperature of the ampule was lowered to room temperature in a natural cooling mode. In this way, single crystals of $SnSb_2Te_4$, with a black color, were successfully prepared and finely powdered in an agate mortar for convenience in high pressure studies. The morphologies of the obtained powders were characterized using SEM images taken on a Hitachi S4800 microscope. The elemental compositions were characterized using an energy dispersive X-ray spectrometer (EDX).

ADXRD studies at high pressures

In situ high pressure angle dispersive XRD (ADXRD) experiments were carried out using a symmetric diamond anvil cell (DAC). The culets of the two diamond anvils were about 300 μm in diameter. The gasket was made of T301 stainless steel. A hole about 50 μm in diameter was drilled at the center of the gasket, serving as the sample chamber. The prepared powders of $SnSb_2Te_4$ were loaded into the sample chamber together with a small chip of ruby, which was used as the pressure indicator[27]. The mixture of methanol and ethanol in a volume ratio of 4:1 was used as the pressure transmitting medium. *In situ* high pressure ADXRD experiments were performed at the high pressure station on the 4W2 beam line of Beijing Synchrotron Radiation Facility (BSRF). The wavelength of the incident monochromatic synchrotron X-ray was 0.6199 Å. The XRD data were recorded using a MAR image plate. The Dioptas package was employed to process the raw XRD data[28]. The full profile indexing and refinements of the diffraction patterns were carried out using the GSAS+EXPGUI package, employing the Le Bail method[29].

Electrical measurements at high pressures and low temperatures

The electrical transport characteristics of $SnSb_2Te_4$ at high pressures and low temperatures (HPLT) were investigated using a symmetric DAC with two 300 μm culet diamond anvils. In order to prevent short circuits between the electrode leads and the gasket, fine powders of Al_2O_3 were employed to cover the T301 stainless steel gasket on one side to form a layered composite gasket. The gasket was initially 250 μm in thickness and pre-indented to about 30 μm. A hole with a diameter of 260 μm was drilled at the center of the indented region. Then, fine powders of Al_2O_3 were filled and compressed in the hole. Finally, a hole with a diameter of 150 μm was drilled at the center of compact Al_2O_3 to serve as the sample chamber, and the sample powders of $SnSb_2Te_4$ were loaded into it. To ensure reliable contact between the electrodes and the sample powders, pressure transmitting medium was avoided in electrical measurements. The pressure was calibrated using either the ruby fluorescence R1 line[27,30,31] or the high frequency edge of the Raman scattering peak of diamond[32] (at low temperatures). Pt wires with a diameter of 4 μm were employed as the electrodes. The electrical resistance of the sample was measured using the traditional four-probe method. The electric voltages and currents involved were measured using a Keithley 2182A nanovoltmeter and 6221 AC and DC sources, respectively. The low temperature conditions were generated and maintained using an integrated low temperature system (Janis PTSHI-950-LT). The sample was compressed under 41 GPa at increments of approximately 2 GPa and cooled down to 5.2 K from the ambient temperature. After each increment, a temperature cycle was performed. The rate of temperature slowly decreased to ensure temperature equilibrium.

Theoretical simulation

Ab initio energetic and electronic calculations of $SnSb_2Te_4$ were performed based on the framework of DFT as implemented in the Vienna *ab initio* simulation package (VASP)[33]. The generalized gradient approximation (GGA) of Perdew-Burke-Ernzerhof (PBE) functional[34] was adopted to describe the exchange-correlation energies. The electron-ion interaction was described using the projector augmented wave (PAW) method[35], considering $5s^25p^2$, $5s^25p^3$, and $5s^25p^4$ as valence electrons for Sn, Sb, and Te atoms. The cutoff energy of the plane waves was set at 900 eV. The fine Monkhorst-Pack[36] *k* meshes with a spacing of $2\pi \times 0.18$ Å^{-1} were adopted in order that the calculated enthalpy were well converged to values with an accuracy higher than 1 meV/atom. The spin-orbit coupling effect was considered in the calculations of the electronic band structures.

RESULTS AND DISCUSSION

Physical characterization under ambient pressure

The crystal structure of $SnSb_2Te_4$ is shown in Figure 1A. Under ambient conditions, the crystal structure of $SnSb_2Te_4$ belongs to the trigonal system with the *R-3m* space group (phase I). In the structure, rocksalt-type building blocks comprising septuple layers (SLs) of alternating cations and anions are stacked along the crystallographic c axis. The SLs, with the ideal sequence of Te_1-Sb-Te_2-Sn-Te_2-Sb-Te_1, are held together through the van der Waals gaps between the hexagonal Te layers terminating the blocks. The hexagonal unit cell includes three SLs. Based on the Le Bail refinement of the XRD patterns of $SnSb_2Te_4$ powders [Figure 1B] using GSAS, the unit cell parameters are determined: a = 4.301 Å and c = 41.598 Å. The results are consistent with those reported previously[37]. The typical scanning electron microscope (SEM) image of the as-prepared $SnSb_2Te_4$ sample is shown in Figure 1C. It shows that the prepared sample consists mainly of flakes with irregular shapes due to vigorous grinding treatment. However, all the flakes show clearly flat basal planes since they were actually broken single crystals. The size of the flakes ranges from 1 to 10 μm. The chemical composition of the sample was measured by energy-dispersive X-ray spectroscopy (EDS). Figure 1D demonstrates that the sample comprises mainly Sn, Sb, and Te elements. In a wide spectrum range (0-10 keV), no signal from any other element is detectable. Through quantitative analysis based on the EDX spectra, the atomic ratio of Sn:Sb:Te is estimated to be 1:2:4, in good agreement with the proposed chemical formula.

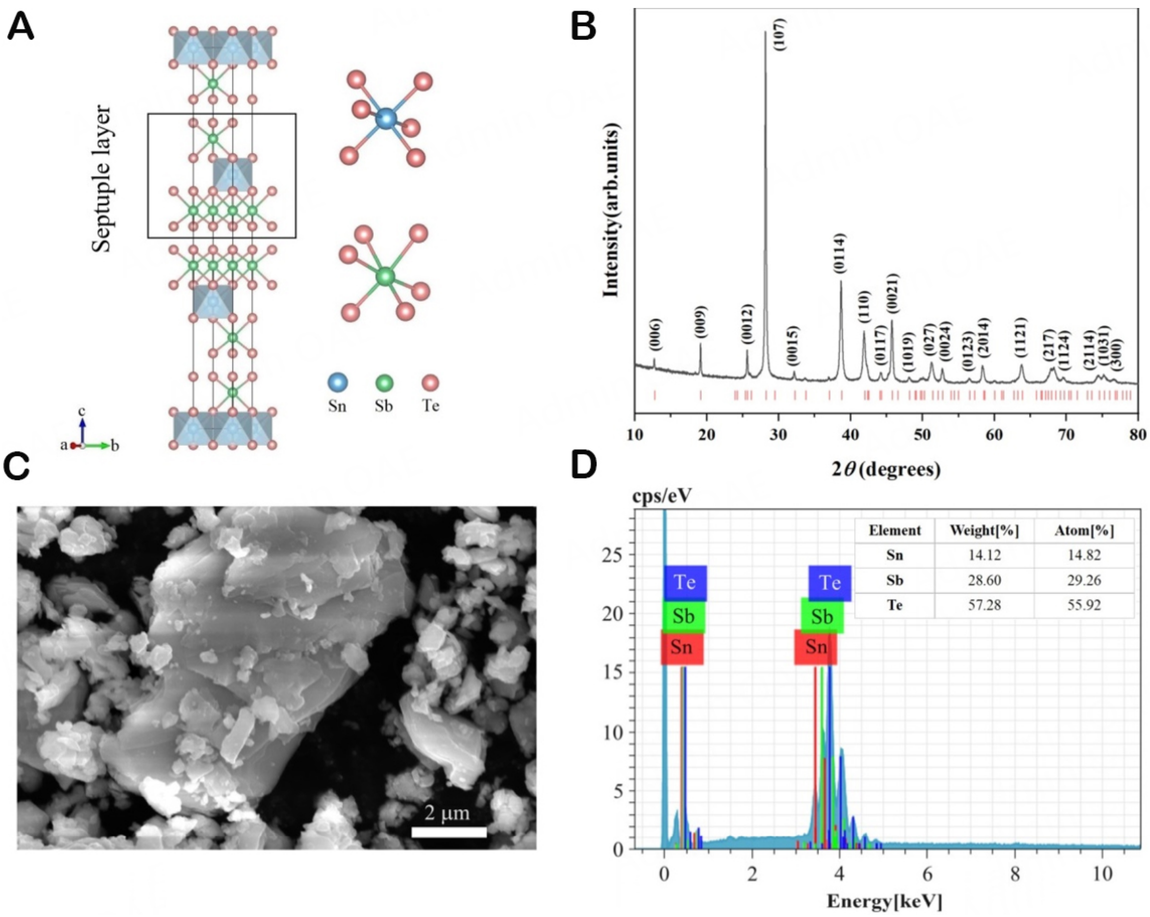

Figure 1. (A) The crystal structure of $SnSb_2Te_4$. The square frame shows a single SL building block. Blue, green, and magenta balls stand for Sn, Sb, and Te atoms. (B) The typical XRD patterns of $SnSb_2Te_4$ powders at ambient pressure. (C) The typical SEM image of the as-prepared $SnSb_2Te_4$ powders. (D) The typical EDX spectra of the as-prepared $SnSb_2Te_4$ powders.

Pressure-induced structural transformations

In the ADXRD studies, it was observed that $SnSb_2Te_4$ experienced three sequential structural phase transitions under compression at 0-45.6 GPa [Figure 2A]. As pressure increased to approximately 6.3 GPa, the emergence of new diffractions (marked with solid circles) indicated that the initial trigonal structure (phase I) lost stability, and a new phase (denoted as phase II) appeared. Phase II was fully established at > 12.9 GPa. It was noteworthy that phase I persisted and coexisted with phase II up to approximately 8.9 GPa. Previous studies on $SnSb_2Te_4$[20] under high pressures demonstrated the pressure-induced decomposition at > 7 GPa. However, our experimental studies did not observe any signs of decomposition [Supplementary Figures 1-3]. To determine the structure of phase II, the pressure-induced phase transition sequences of the binary VA-VIA compound counterparts of $SnSb_2Te_4$, such as Bi_2Te_3[38,39], Bi_2Se_3[40], Sb_2Te_3[41], Sb_2Se_3[42], and Sb_2S_3[17,43], and the related ternary ones, such as Bi_2Te_2Se[44] and $SnBi_2Te_4$[15], were considered. Therefore, phase II was assigned to a *C2/m* space group. The assignment could be validated based on the Le Bail refinement of the ADXRD patterns [Figure 3A]. The reflections from phase II can be indexed to the *C2/m* structure, yielding the lattice parameters summarized in Table 1. As the pressure further increased to 15.5 GPa, additional diffraction peaks appeared in the ADXRD patterns [marked with solid diamonds in Figure 2A, indicating the emergence of another new phase (phase III). Phase III remained stable at 15.5-40.2 GPa. Under the stable pressure range, phase III coexisted with phase II and/or phase IV. Owing to the complicacy of the ADXRD profiles, it becomes difficult to determine the exact crystal structure and

Table 1. The lattice parameters of $SnSb_2Te_4$ phases at 3.2, 8.9, 15.5, and 44.7 GPa, derived from Le Bail refinements, as shown in Figure 3

Phase	Space group	Pressure	Lattice parameters (Å)	Volume (Å^3)
phase I	*R-3m*	3.1 GPa	$a = b = 4.224$ (3) $c = 39.742$ (7)	614.18 (3)
phase II	*C2/m*	8.9 GPa	$a = 14.253$ (2) $b = 4.128$ (6) $c = 17.120$ (2) $\beta = 149.059$ (3)	519.04 (7)
phase III	*C2/c*	15.5 GPa	a = 10.137 (9) $b = 7.105$ (3) $c = 10.660$ (7) $\beta = 136.320$ (5)	530.30 (5)
phase IV	*Im-3m*	44.7 GPa	$a = b = c = 3.459$ (6)	41.10 (6)

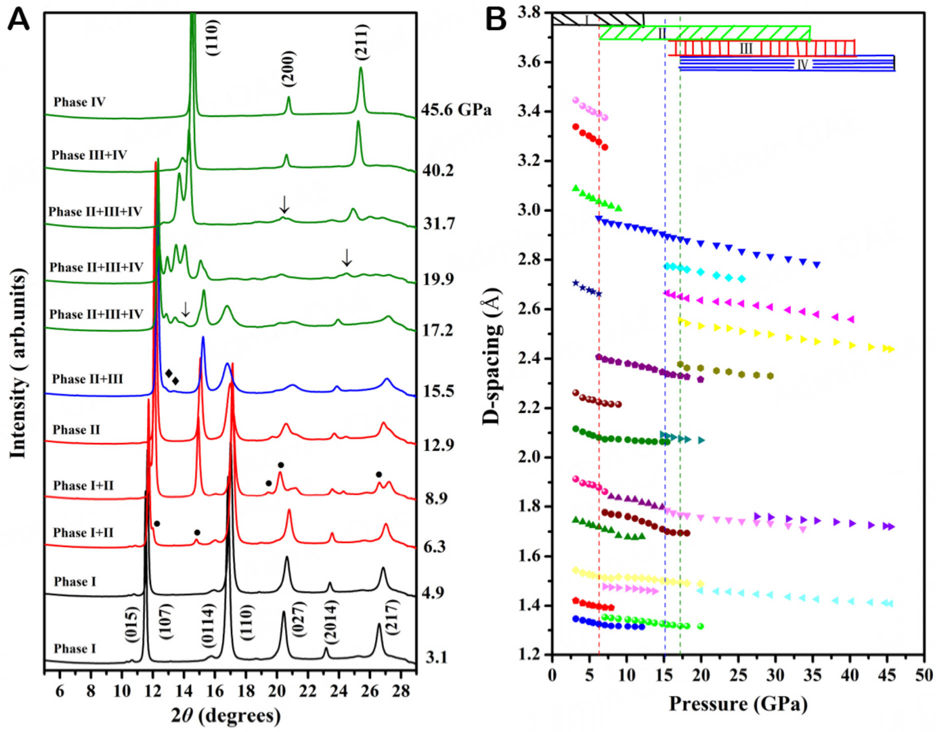

Figure 2. The structural evolution of $SnSb_2Te_4$ at high pressures. (A) The typical ADXRD patterns of $SnSb_2Te_4$ acquired at various high pressures and room temperature. The solid circles, diamonds, and arrows are used to indicate the emerging diffractions of phases II, III, and IV. (B) The pressure-dependent evolution of the *d*-spacings of $SnSb_2Te_4$. The pressure ranges in which the structural phases exist are labeled with vertical dash lines. Across the phase transition pressures, the slopes of the variation curves of the *d*-spacings change discontinuously.

lattice parameters of phase III. However, similar to the assignment of phase II, phase III might be tentatively assigned to a *C2/c* structure [Figure 3B]. With further increase of the pressure to 17.2 GPa, new diffraction peaks started to emerge, which were marked with black arrows in Figure 2A. They indicated the onset of the third phase transformation into phase IV. Phase IV at high pressures can be indexed to the body-centered cubic structure (space group No.229, *Im-3m*) with the unit cell parameter of a = 3.459 Å. Phase IV remained stable up to 45.6 GPa, the highest pressure achieved herein. Le Bail fitting for the XRD patterns at various pressures was shown in Figure 3A-D.

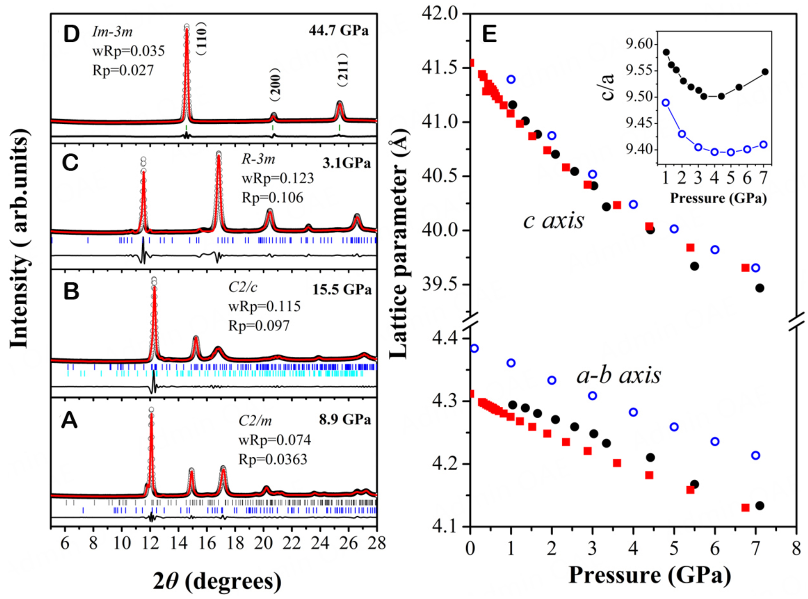

Figure 3. The full profile diffraction patterns of $SnSb_2Te_4$ at (A) 8.9, (B) 15.5, (C) 3.1 and (D) 44.7 GPa. The solid lines in red represent the fitting curves of the diffraction patterns of the involved structures via Le Bail refinements, and open circles represent the experimental data points. The solid lines in black at the bottom represent the residual deviations between the fitted and the observed intensities. The vertical bars indicate the theoretical peak positions of the involved structural phases. The diffraction patterns in (A) comprise a mixture of phases I and II. Those in (B) comprise a mixture of phases II and III. (E) The pressure dependence of the lattice parameters for phase I. The lattice parameters are indicated by squares, solid circles, and hollow circles, corresponding to the data reported by Sans *et al.*[20] and those obtained experimentally and theoretically in the present study. The inset shows the pressure dependence of the axial ratio *c/a*.

In the *bcc* (*Im-3m*) structure, it was demanded by symmetry that only one inequivalent atomic position at the 2*a* Wyckoff site was allowed. As a result, in phase IV of $SnSb_2Te_4$, the distribution of Sn, Sb, and Te atoms was disordered, and they had to share the *bcc* lattice sites in a random manner. Hence, an Sn-Sb-Te substitutional solid solution is formed. The similar phenomena have also been observed in the high pressure-induced substitutional solid solution phases in Bi_2Te_3, Sb_2Te_3, and Sb_2Se_3. The formation of the high pressure substitutional solid solutions can be roughly explained in terms of atomic size and electronegativity. As pressure was gradually increased, these parameters for different atoms tended to become almost homogenous. Thus, it turned out to be possible for them to form substitutional solid solutions at high pressures. Moreover, the pressure-dependent variation trends of the lattice *d*-spacings [Figure 2B] and the volume [Supplementary Figure 4] indicated additional signs of the phase transitions. Thus, based on the aforementioned results and discussion, for $SnSb_2Te_4$, the pressure-induced structural phase transition sequence might be *R-3m* → *C2/m* →*C2/c* → disordered *Im-3m.*

Several factors may contribute to the broadening of the diffraction peaks in high pressure XRD patterns. First, the non-hydrostatic stress in the samples may lead to systematic broadening and weakening of the diffraction peaks with increasing pressure. Second, amorphization, if it occurs, may lead to diffuse diffractions with large width and low intensity. In the third place, the overlapping of the diffraction peaks of coexisting phases may exhibit broad convolutional profiles when they have similar *d*-spacings. In this work, coexistence of phases II, III, and IV may be the major origin of the broadening of the diffraction peaks around 15-17 GPa. The occurrence of amorphization was hardly possible since the diffraction peaks in the low-angle range remained sharp and strong.

Pressure-induced electron topological transition

The pressure dependences of the experimental and theoretical lattice parameters and the axial ratio *c/a* of the initial phase are illustrated in Figure 3E. A minimum can be observed in the variation curve of *c/a* at approximately 3 GPa. Generally, it suggests the occurrence of the electron topological transition (ETT) near this pressure. These experimental results agree well with our theoretical calculations. The abnormal variation in the *c/a* ratio with pressure is considered as a good indicator of ETT. It is caused by the anomalous compression behavior of the *a* axis under high pressures, which results in a profound change in compressibility during ETT[41]. The topological transition of electrons related to electrical transportation in $SnSb_2Te_4$ can be visualized based on the first-principles calculations of the electron energy bands [Figure 4]. Under ambient conditions, the minimum conduction band (MCB) and maximum valence band (MVB) appear at the high symmetric point (A) of the Brillouin zone (BZ). The calculation results of the density of states (DOS) indicate that Te mainly contributes to the MVB, and Sn contributes to the MCB. In agreement with previous reports[22], $SnSb_2Te_4$ is a direct band gap semiconductor. However, the narrow band gap of 0.02 eV indicates that $SnSb_2Te_4$ may behave as a metal at room temperature owing to self-doping effects.

Under compression, the repulsion between the electron states of Te and Sn considerably increases with pressure. As a result, the positions of the MCB and MVB change substantially. $SnSb_2Te_4$ becomes an indirect band gap semiconductor. At 2.0 GPa, the MVB moves to a high symmetric point along the Γ-M direction in the BZ, with the complex contributions of Sn, Sb, and Te. Along the Γ-M direction near the Γ point, at least three dispersive branches compete for the MCB. The indirect band gap decreases with an increase in pressure. ETT occurs when an extreme of the electronic band structure, which is associated with the Van Hove singularity in the DOS, exceeds the Fermi energy (EF) and leads to a strong redistribution of the EDOS near the EF[43]. In one of the previous studies that reported the analysis of $SnBi_2Te_4$ under high pressures, a discontinuous change in the *c/a* ratio under pressure was found to be related to the inflection point of electrical resistance at 2 GPa, which implies the occurrence of ETT in phase I[15]. Moreover, ETT existed based on the phonon spectrum measurements observed in the parent binary compound, i.e., Sb_2Te_3[45], and the compounds of the A_2B_3 chalcogenide series, e.g., Bi_2Se_3, Sb_2S_3, and Bi_2Te_3[40,43,46].

Pressure-induced superconductivity

The temperature dependence of the electrical resistance of $SnSb_2Te_4$ was obtained at 12.3-41 GPa [Figure 5A]. At < 12.3 GPa, the conducting behavior is characteristic of a metal without the marked signature of superconductivity down to the lowest temperature measured. When the pressure increased to 12.3 GPa, superconducting transition with a T_c value of approximately 5.2 K was observed [Figure 5A]. When the pressure increased to 13.8 GPa, the decrease in electrical resistance became more evident, and the zero-resistance state was fully realized. Moreover, T_c increased rapidly with pressure. Herein, the zero-resistance critical temperature (Tc^{zero}) and the onset temperature of superconducting transition (Tc^{onset}) were determined. At > 25.1 GPa, there was a little difference between Tc^{zero} and Tc^{onset}, hovering near a width of about 1 K. Herein, the maximum value of *Tc* was calculated to be approximately 8.2 K at 17.1 GPa, very close to those reported for $SnBi_2Te_4$ (8.9 K)[15] and $GeSb_2Te_4$ (8 K)[25] under pressure. A comparison of T_c and critical pressures for other TS candidates is shown in Supplementary Table 1.

Figure 5B shows the superconducting phase diagram of the $SnSb_2Te_4$ powders. Two regions can be distinguished based on the changes in *Tc* with elevated pressure. At 12.3-17.1 GPa, in which phases II and III coexist, Tc^{onset} increases monotonically with pressure. The steep slope indicates the strong pressure-induced enhancement of superconductivity. The pressure dependence of *Tc* at the aforementioned pressure range is similar to that reported in the previous study[22]. It can be concluded that the positive pressure dependence on *Tc* observed under pressures of up to 17.1 GPa is correlated to monoclinic *C2/m* phase II. For Sb_2Te_3[9] or the binary VA-VIA compound counterparts of $SnSb_2Te_4$, the evolution of T_C as a function of

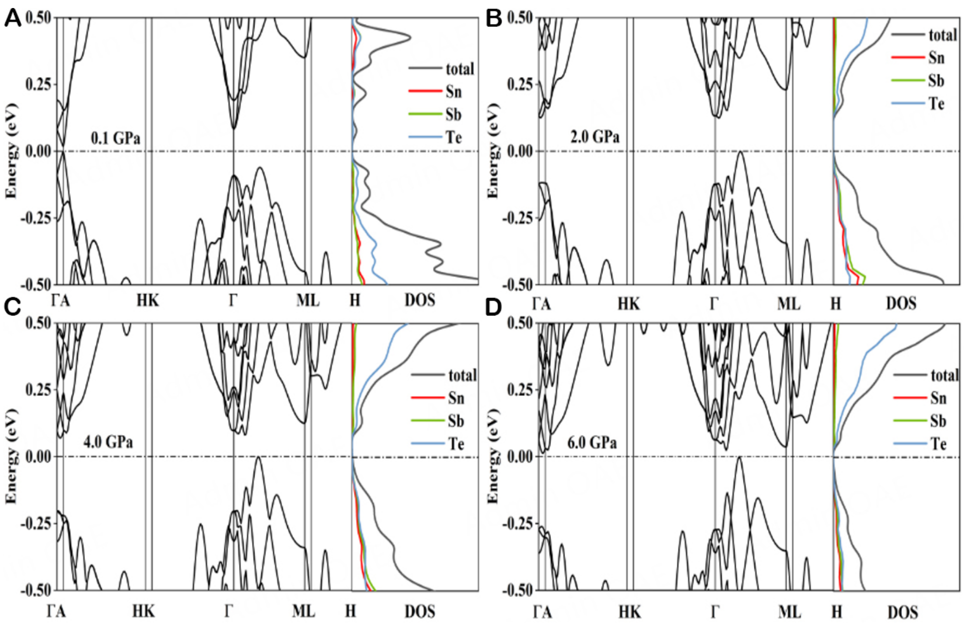

Figure 4. Electronic band structures of $SnSb_2Te_4$ at (A) 0.1, (B) 2.0, (C) 4.0, and (D) 6.0 GPa in the presence of spin–orbit coupling.

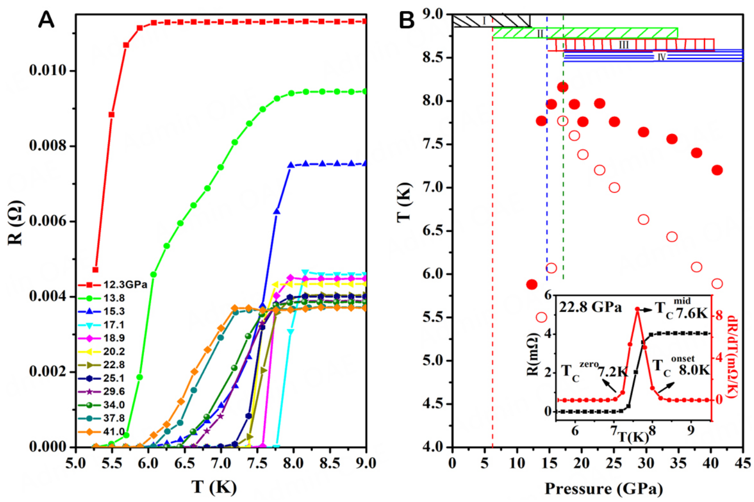

Figure 5. (A) The temperature dependence of the electrical resistance of $SnSb_2Te_4$ at various high pressures. (B) The pressure dependence of the critical temperatures Tc^{onset} and Tc^{zero} of $SnSb_2Te_4$. The solid and hollow circles stand for Tc^{onset} and Tc^{zero}, respectively. The inset depicts the differential curve *dR/dT* of the electrical resistance near *Tc*. The symbols Tc^{onset}, Tc^{mid}, and Tc^{zero} are defined accordingly. Tc^{onset} refers to the temperature at which the drop in electrical resistance begins; Tc^{zero} refers to the temperature at which electrical resistance decreases to zero; Tc^{mid} refers to the temperature at which the maximum of the *dR/dT* curve occurs.

pressure indicates a positive trend as well. At > 17.1 GPa, the sharp decrease in and the negative pressure dependence of *Tc* indicate the presence of a new superconducting phase [Figure 5B]. T_C monotonically decreases to 7.2 K at 41.0 GPa. The new superconducting phase corresponds to phase IV (the substitutional solid solution with the *bcc* structure), which exists at > 17.1 GPa and room temperature. Similar trends in the pressure effect on T_C for the substitutional solid solution phases of Bi_2Te_3[47], Bi_4Te_3[48], and $SbBi_2Te_4$[15] are also observed. For these materials, superconductivity is depressed by high pressure. As a whole, pressure-driven superconductivity in $SnSb_2Te_4$ relates closely to the structural phase transitions. The obtained phase diagram reveals a relationship between the structural transition and the appearance of superconductivity.

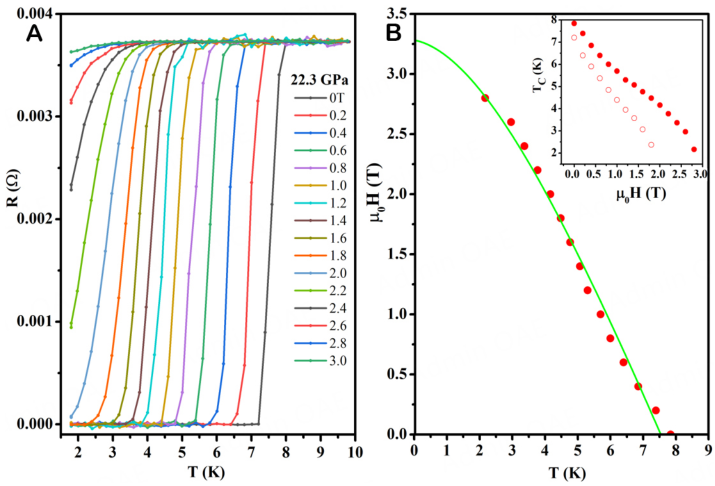

Figure 6. (A) The temperature dependence of the electrical resistance under various external magnetic fields with the pressure held constant at 22.3 GPa. (B) The temperature dependence of the reduced upper critical field $\mu_0 H(T)$ (red circles) and the fitting curve according to the WHH formula (green line). The inset shows the dependence of T_c on the external magnetic field. The solid and hollow circles stand for Tc^{onset} and Tc^{zero}, respectively.

To ensure the superconducting transition illustrated in Figure 5, we performed electrical resistance measurements near the critical temperature at a varying external magnetic field. The results were shown in Figure 6A with the pressure fixed at 22.3 GPa. It is clear that T_c decreased with increasing magnetic field, confirming that the transition is really superconductive. It is also shown that, with and without a magnetic field, the drop in the electrical resistance is very sharp, indicating bulk and homogeneous occurrence of superconductivity. Figure 6B shows the plot of the temperature dependence of the reduced upper critical field $\mu_0 H(T)$ (red circles). The data points are fitted to the Werthdamer-Helfand-Hohenberg (WHH) formula[49]

$$\mu_0 H_{c2}(T) = \frac{\mu_0 H_{c2}(0)}{0.693}\left(\left(1-\frac{T}{T_C}\right)-0.153\left(1-\frac{T}{T_C}\right)^2-0.152\left(1-\frac{T}{T_C}\right)^4\right),$$

and the obtained fitting curve (green line) was also shown in Figure 6B. Through extrapolation of the fitting curve, the upper critical field $H_{c2}(0)$ was estimated to be 3.3 Tesla for $H_{||c}$. In the inset of Figure 6B, the variations of the critical temperatures T_C^{onset} and T_C^{zero} with magnetic field H were demonstrated.

CONCLUSIONS

In summary, as a promising candidate material for topological quantum states, $SnSb_2Te_4$ has attracted considerable research interest owing to its structural and electric transport behaviors, which are related to not only fundamental sciences but also potential applications in spintronics and quantum technologies. Herein, powdered samples of $SnSb_2Te_4$ were subjected to severe compression using DAC techniques. Similar to its binary end-member, i.e., Sb_2Te_3, $SnSb_2Te_4$ experienced structural phase transformations under high pressures in the following sequence: *R-3m* → *C2/m* → *C2/c* → disordered *Im-3m*. The focus was on the disordered site in high-pressure phases; i.e., in all the cases, the lattice sites were randomly occupied by substituent atoms, i.e., Sn, Sb, and Te. Such structural features, which are consistent with its binary and ternary chalcogenide counterparts, might enable the pressure-driven superconductivity of materials in this family. In this case study on $SnSb_2Te_4$, two distinct superconducting states, bulk and homogeneous, were observed at high pressures; they were closely related to the high-pressure monoclinic *C2/m* and cubic *Im-3m* phases, respectively. This study offers the opportunity for a deeper comprehension of the correlations between the metastable structural phases and the pressure-induced superconducting states of $SnSb_2Te_4$, which can clarify the general physical phenomenon giving rise to superconducting states in potential candidates for topological quantum materials.

DECLARATIONS

Authors' contributions

Conceptualization, investigation, writing - review & editing: Ma Y
Investigation: Wang H
Investigation, writing - original draft: Li R
Methodology: Liu H
Conceptualization, writing-review & editing: Zhang J
Synthesis: Wang X
Synthesis, formal analysis: Jing Q
Investigation: Wang X, Dong W, Chen J, Wu B
Validation, investigation: Han Y
Investigation, writing-review & editing: Zhou D
Validation, conceptualization: Gao C

Availability of data and materials

The authors declare that the main data supporting the findings of this study are contained within the paper and its associated Supplementary Materials. All other relevant data are available from the corresponding author upon reasonable request.

Financial support and sponsorship

This work was supported by the National Natural Science Foundation of China (Grant No. 11974130, No. 12004015, No. 11874028, and No. 11704044). High pressure XRD experiments were performed at the 4W2 beamline of Beijing Synchrotron Radiation Facility and BL15U1 beamline of Shanghai Synchrotron Radiation Facility. Additionally, we acknowledge support from the User Experiment Assist System of Shanghai Synchrotron Radiation Facility (SSRF).

Conflicts of interest

All authors declared that there are no conflicts of interest.

Ethical approval and consent to participate

Not applicable.

Consent for publication

Not applicable.

REFERENCES

1. Qi XL, Zhang SC. Topological insulators and superconductors. *Rev Mod Phys* 2011;83:1057-110. DOI
2. Drozdov AP, Eremets MI, Troyan IA, Ksenofontov V, Shylin SI. Conventional superconductivity at 203 kelvin at high pressures in the sulfur hydride system. *Nature* 2015;525:73-6. DOI PubMed
3. Bednorz JG, Müller KA. Possible highT_c superconductivity in the Ba-La-Cu-O system. *Z Phys B Condens Matter* 1986;64:189-93. DOI
4. Schilling A, Cantoni M, Guo JD, Ott HR. Superconductivity above 130 K in the Hg-Ba-Ca-Cu-O system. *Nature* 1993;363:56-8. DOI

5. Vergniory MG, Menshchikova TV, Eremeev SV, Chulkov EV. Bulk and surface electronic structure of $SnBi_4Te_7$ topological insulator. *Appl Surf Sci* 2013;267:146-9. DOI
6. Vergniory MG, Menshchikova TV, Silkin IV, Koroteev YM, Eremeev SV, Chulkov EV. Electronic and spin structure of a family of Sn-based ternary topological insulators. *Phys Rev B* 2015;92:045134. DOI
7. Souma S, Eto K, Nomura M, et al. Topological surface states in lead-based ternary telluride $Pb(Bi_{1-x}Sb_x)_2Te_4$. *Phys Rev Lett* 2012;108:116801. DOI
8. Neupane M, Xu SY, Wray LA, et al. Topological surface states and dirac point tuning in ternary topological insulators. *Phys Rev B* 2012;85:235406. DOI
9. Zhu J, Zhang JL, Kong PP, et al. Superconductivity in topological insulator Sb_2Te_3 induced by pressure. *Sci Rep* 2013;3:2016. DOI PubMed PMC
10. Zhang JL, Zhang SJ, Weng HM, et al. Pressure-induced superconductivity in topological parent compound Bi_2Te_3. *Proc Natl Acad Sci USA* 2011;108:24-8. DOI PubMed PMC
11. Kirshenbaum K, Syers PS, Hope AP, et al. Pressure-induced unconventional superconducting phase in the topological insulator Bi_2Se_3. *Phys Rev Lett* 2013;111:087001. DOI
12. Polvani DA, Meng JF, Chandra Shekar NV, Sharp J, Badding JV. Large improvement in thermoelectric properties in pressure-tuned *p*-type $Sb_{1.5}Bi_{0.5}Te_3$. *Chem Mater* 2001;13:2068-71. DOI
13. Shelimova LE, Karpinskii OG, Zemskov VS, Konstantinov PP. Structural and electrical properties of layered tetradymite-like compounds in the GeTe-Bi_2Te_3 and GeTe-Sb_2Te_3 systems. *Inorg Mater* 2000;36:235-42. DOI
14. Shelimova LE, Konstantinov PP, Karpinsky OG, Avilov E, Kretova M, Zemskov V. X-ray diffraction study and electrical and thermal transport properties of the nGeTe·mBi_2Te_3 homologous series compounds. *J Alloys Compd* 2001;329:50-62. DOI
15. Li R, Liu G, Jing Q, et al. Pressure-induced superconductivity and structural transitions in topological insulator $SnBi_2Te_4$. *J Alloys Compd* 2022;900:163371. DOI
16. Vilaplana R, Sans JA, Manjón FJ, et al. Structural and electrical study of the topological insulator $SnBi_2Te_4$ at high pressure. *J Alloys Compd* 2016;685:962-70. DOI
17. Wang Y, Ma Y, Liu G, et al. Experimental observation of the high pressure induced substitutional solid solution and phase transformation in Sb_2S_3. *Sci Rep* 2018;8:14795. DOI PubMed PMC
18. Xi X, Ma C, Liu Z, et al. Signatures of a pressure-induced topological quantum phase transition in BiTeI. *Phys Rev Lett* 2013;111:155701. DOI
19. Niesner D, Otto S, Hermann V, et al. Bulk and surface electron dynamics in a *p*-type topological insulator $SnSb_2Te_4$. *Phys Rev B* 2014;89:081404. DOI
20. Sans JA, Vilaplana R, da Silva EL, et al. Characterization and decomposition of the natural van der waals $SnSb_2Te_4$ under compression. *Inorg Chem* 2020;59:9900-18. DOI
21. Chandra S, Sunil J, Dutta P, et al. Evidence of pressure-induced multiple electronic topological transitions in BiSe. *Mater Today Phys* 2023;30:100956. DOI
22. Song P, Matsumoto R, Hou Z, et al. Pressure-induced superconductivity in $SnSb_2Te_4$. *J Phys Condens Matter* 2020;32:235901. DOI
23. Zhao X, Zhang K, Qi J, et al. Low-pressure-driven barocaloric effects at colinear-to-triangular antiferromagnetic transitions in $Mn_{3-x}Pt_{1+x}$. *Microstructures* 2023;3:2023022. DOI
24. Matsumoto R, Hou Z, Hara H, et al. Two pressure-induced superconducting transitions in $SnBi_2Se_4$ explored by data-driven materials search: new approach to developing novel functional materials including thermoelectric and superconducting materials. *Appl Phys Express* 2018;11:093101. DOI
25. Greenberg E, Hen B, Layek S, et al. Superconductivity in multiple phases of compressed $GeSb_2Te_4$. *Phys Rev B* 2017;95:064514. DOI
26. Matsumoto R, Hou Z, Nagao M, et al. Data-driven exploration of new pressure-induced superconductivity in $PbBi_2Te_4$. *Sci Technol Adv Mater* 2018;19:909-16. DOI PubMed PMC
27. Mao HK, Xu J, Bell PM. Calibration of the ruby pressure gauge to 800 kbar under quasi-hydrostatic conditions. *J Geophys Res* 1986;91:4673-6. DOI
28. Prescher C, Prakapenka VB. *DIOPTAS*: a program for reduction of two-dimensional X-ray diffraction data and data exploration. *High Pressure Res* 2015;35:223-30. DOI
29. Toby BH. *EXPGUI*, a graphical user interface for *GSAS*. *J Appl Cryst* 2001;34:210-3. DOI
30. Nakano K, Akahama Y, Ohishi Y, Kawamura H. Ruby scale at low temperatures calibrated by the NaCl gauge: wavelength shift of ruby R1 fluorescence line at high pressure and low temperature. *Jpn J Appl Phys* 2000;39:1249. DOI
31. Xu LW, Che RZ, Jin CQ. Measurement of R line fluorescence in ruby using the diamond anvil cell at low temperature. *Chin Phys Lett* 2000;17:555-7. DOI
32. Akahama Y, Kawamura H. Pressure calibration of diamond anvil Raman gauge to 410 GPa. *J Phys Conf Ser* 2010;215:012195. DOI
33. Kresse G, Furthmüller J. Efficient iterative schemes for ab initio total-energy calculations using a plane-wave basis set. *Phys Rev B Condens Matter* 1996;54:11169-86. DOI PubMed
34. Perdew JP, Burke K, Ernzerhof M. Generalized gradient approximation made simple. *Phys Rev Lett* 1996;77:3865-8. DOI PubMed
35. Blöchl PE. Projector augmented-wave method. *Phys Rev B Condens Matter* 1994;50:17953-79. DOI PubMed
36. Monkhorst HJ, Pack JD. Special points for brillouin-zone integrations. *Phys Rev B* 1976;13:5188-92. DOI
37. Oeckler O, Schneider MN, Fahrnbauer F, Vaughan G. Atom distribution in $SnSb_2Te_4$ by resonant X-ray diffraction. *Solid State Sci*

2011;13:1157-61. DOI

38. Einaga M, Ohmura A, Nakayama A, Ishikawa F, Yamada Y, Nakano S. Pressure-induced phase transition of Bi_2Te_3 to a bcc structure. *Phys Rev B* 2011;83:092102. DOI
39. Nakayama A, Einaga M, Tanabe Y, Nakano S, Ishikawa F, Yamada Y. Structural phase transition in Bi_2Te_3 under high pressure. *High Pressure Res* 2009;29:245-9. DOI
40. Vilaplana R, Santamaría-pérez D, Gomis O, et al. Structural and vibrational study of Bi_2Se_3 under high pressure. *Phys Rev B* 2011;84:184110. DOI
41. Ma Y, Liu G, Zhu P, et al. Determinations of the high-pressure crystal structures of Sb_2Te_3. *J Phys Condens Matter* 2012;24:475403. DOI
42. Efthimiopoulos I, Zhang JM, Kucway M, Park C, Ewing RC, Wang Y. Sb_2Se_3 under pressure. *Sci Rep* 2013;3:2665. DOI PubMed PMC
43. Sorb YA, Rajaji V, Malavi PS, et al. Pressure-induced electronic topological transition in Sb_2S_3. *J Phys Condens Matter* 2016;28:015602. DOI
44. Nielsen MB, Parisiades P, Madsen SR, Bremholm M. High-pressure phase transitions in ordered and disordered Bi_2Te_2Se. *Dalton Trans* 2015;44:14077-84. DOI PubMed
45. Gomis O, Vilaplana R, Manjón FJ, et al. Lattice dynamics of Sb_2Te_3 at high pressures. *Phys Rev B* 2011;84:174305. DOI
46. Vilaplana R, Gomis O, Manjón FJ, et al. High-pressure vibrational and optical study of Bi_2Te_3. *Phys Rev B* 2011;84:104112. DOI
47. Zhang SJ, Zhang JL, Yu XH, et al. The comprehensive phase evolution for Bi_2Te_3 topological compound as function of pressure. *J Appl Phys* 2012;111:112630. DOI
48. Jeffries JR, Lima Sharma AL, Sharma PA, et al. Distinct superconducting states in the pressure-induced metallic structures of the nominal semimetal Bi_4Te_3. *Phys Rev B* 2011;84:092505. DOI
49. Werthamer NR, Helfand E, Hohenberg PC. Temperature and purity dependence of the superconducting critical field, H_{c2}. III. electron spin and spin-orbit effects. *Phys Rev* 1966;147:295. DOI